Density Functional Theory Study of CO Adsorption on Fe_5C_2(001), -(100), and -(110) Surfaces

Dong-Bo Cao,[†] Fu-Qiang Zhang,[†] Yong-Wang Li,[†] and Haijun Jiao*[,†,‡]

State Key Laboratory of Coal Conversion, Institute of Coal Chemistry, Chinese Academy of Sciences, Taiyuan 030001, People's Republic of China, and Leibniz-Institut für Organische Katalyse an der Universität Rostock e.V., Buchbinderstrasse 5-6, 18055 Rostock, Germany

Received: February 5, 2004; In Final Form: April 4, 2004

Density functional theory calculations have been carried out to study CO adsorption on the (001), (100), and (110) surfaces of Fe_5C_2, which are considered as active catalysts in Fischer−Tropsch synthesis. It is found that CO prefers to adsorb at three 3-fold sites (three iron atoms) on the three surfaces at low coverage with maximum adsorption energies of −2.10, −2.21, and −2.34 eV, respectively. The adsorption energy of CO adsorbed around surface carbon atoms on (001) is higher than that on (110) by up to 0.94 eV. The difference is attributed to the C 2p−Fe 3d bands that mainly lie at the lower energy level on bare (110) than that on bare (001). This indicates that the surface Fe−C bonds on (110) are stronger than those on (001), which in turn hinders local CO adsorption on (110). In contrast to (001) and (110), a monolayer of the (100) surface only consists of iron atoms. The adsorption energy at low coverage on (100) is similar to those on (001) and (110), but the highest at high coverage among all surfaces. These results indicate the diversity of the atomic structure on the underlying Fe_5C_2 surface site. Apart from the (100) surface at high coverage, other surfaces may play dominant roles when practical working conditions permit.

Introduction

Iron-based catalysts are widely used in the industrial Fischer−Tropsch synthesis (FTS) processes,[1] which become increasingly important especially for liquid fuel production under the background of the predicted lack of oil supply. In the course of FTS reactions, an iron-based catalyst is naturally exposed to the syngas ($CO + H_2$) environment that maintains the stable existence of iron carbides.[1] Generally, there are many types of carbides coexisting on a working iron-based catalyst,[2−16] and among them, the most representative one is the Hägg iron carbide (Fe_5C_2). Transmission electron microscopy, X-ray analysis, and Mössbauer spectroscopy indicate that the highly dispersed Fe_5C_2 is responsible for the high FTS activity.[3−10] It has been suspected that the active phase of FTS is a mixture of χ- and ϵ-iron carbides and a small amount of α-Fe,[17] and Fe_2O_3, the catalyst precursor, is transformed to the metastable Fe_3O_4, and then to the amorphous carbon-rich iron carbides during the catalyst reduction and FTS reaction processes.[2,5,18]

The complexity of the coexisting phases on the catalyst surface and the reaction nature of a real FTS system have led to little possibility for the detailed definition and understanding of the active phases with the available analytical methods.[12,16,17,19,20] Nevertheless, experimental studies have come to several general conclusions that have guided the further development of a workable catalyst to some extent: (1) the formation of a reduced active phase from the iron oxide precursor (Fe_2O_3) is essential for the FTS reactions; (2) carbide-phase formation is very important for a stable FTS operation; (3) an obvious correlation between the intensity of the Fe_5C_2 phase in Mössbauer measurements and the FTS activity exists despite the complexity;[3,6,10] (4) CO dissociation is an important step; (5) the carbon of CO and from the carbide phases can undergo exchanges; (6) the products from simple CO and H_2 via FTS are complex, namely, the dominant straight chain *n*-alkenes and alkanes, the small amount of branched iso products, and the small amount of diverse oxygenates.

On one hand, the research and development of a sufficient FTS catalyst and the corresponding process greatly demand a better understanding of the detailed mechanism, which can in turn serve for a better control of activity and selectivity, and also provide the basis for the engineering of the kinetics of a specific FTS process. On the other hand, it is rather difficult to detect the microscopic reaction pathways over the catalyst surfaces under the dramatic real working conditions. The current mechanistic understanding is mainly on the basis of indirect evidence, for example, the existence of surface carbon species (C, CH, CH_2, CH_3, and C_xH_y) detected experimentally.[21,22] For FTS over iron-based catalysts, despite numerous experiments verifying the Fe_5C_2 phase to be one of the active phases, a detailed mechanism and quantitative estimation of the structure and electronic properties of the Fe_5C_2 surface are totally lacking. Alternatively, recent development and advances in quantum chemistry and quantum mechanics can provide fairly accurate estimations of the changes of the structures and energies of molecules on the catalyst surfaces.

CO adsorption on transition-metal surfaces is of technological importance because of the potential use of FTS in the production of hydrocarbons.[1,23] Both experimental and theoretical studies indicate CO adsorption to be likely dissociative on the left side of the first-row transition metals up to Fe, while it is molecular on the right side from Co.[24−29] The location of the adsorbed CO on surfaces is likely at the top, 2-fold, 3-fold, and 4-fold sites. The C−O axis of the chemisorbed CO can be parallel,

* To whom correspondence should be addressed. E-mail: hjiao@ifok.uni-rostock.de.

[†] Chinese Academy of Sciences.

[‡] Leibniz-Institut für Organische Katalyse an der Universität Rostock e.V.

10.1021/jp049470w CCC: $27.50 © 2004 American Chemical Society
Published on Web 05/29/2004

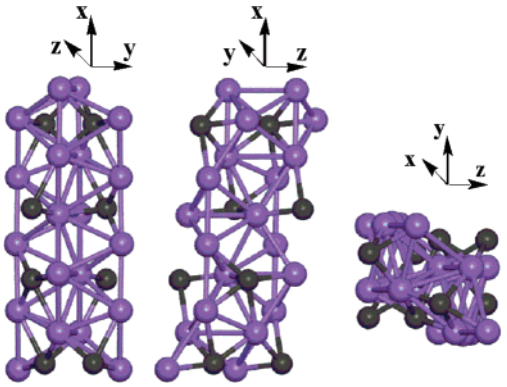

Figure 1. Schematic unit cell of Fe_5C_2 (purple, Fe atom; gray, C atom).

perpendicular, and tilted.[30−37] A theoretical study suggests that the defect sites (surface steps and kinks) play a critical role in catalytic reactions.[38] Jenkins et al.[39] investigated CO adsorption at a monolayer (ML) coverage of 1/2 on the stepped Pt(211) and Ni(211) surfaces with the density functional theory (DFT) method, and the computed adsorption energies are −2.38 and −2.67 eV, respectively. Using the DFT method, Sholl et al.[40] studied CO chemisorption on the flat and stepped Ni surfaces, and the adsorption energy on the steps is higher than on the flat surfaces by 0.13 eV. Similarly, the CO adsorption energy on the stepped and kinked Pt surfaces is higher than on the flat terraces by 0.7 and 1.0 eV with the DFT method,[41] respectively.

For the cases of FTS over iron-based catalysts, there has been little theoretical work done on the most representative active phase, Fe_5C_2.[3−10] As the first step to understand FTS catalysis on such a phase, we carried out detailed DFT calculations to investigate CO adsorption on the (001), (100), and (110) surfaces of Fe_5C_2. We also discussed the bonding mechanism of CO on each of these three surfaces by examining the local density of states (LDOS) for the adsorbed species.

Methods and Models

DFT calculations within the generalized gradient approximation (GGA)[42] were carried out to study CO adsorption on the Fe_5C_2 surfaces. All calculations were carried out by using the Cambridge Sequential Total Energy Package (CASTEP).[43] Ionic cores were described by the ultrasoft pseudopotential,[44] and the Kohn−Sham one-electron states were expanded in a plane wave basis set up to 340 eV. The error of the adsorption energy at the level of cutoff between 300 and 340 eV was less than 0.02 eV. A Fermi smearing of 0.1 eV was utilized. Brillouin zone integration was approximated by a sum over special *k* points chosen using the Monhorst−Pack scheme.[45] The pseudopotential with partial core was used in spin-polarized calculations to include nonlinear core corrections.[46] Spin polarization having a major effect on the adsorption energies for a magnetic system[47−50] was included in the calculations for the superparamagnetic Fe_5C_2[51] to correctly account for its magnetic properties. Without counting the adsorbate, the vacuum between the slabs was set to span a range of 10 Å to ensure no significant interaction between the slabs. The convergence criteria for the structure optimization and energy calculation were set to (a) a SCF tolerance of 2.0×10^{-6} eV/atom, (b) an energy tolerance of 2.0×10^{-5} eV/atom, (c) a maximum force tolerance of 0.05 eV/Å, and (d) a maximum displacement tolerance of 2.0×10^{-3} Å. We used the Molarch$^+$ program[52] to generate the molecular graphics.

Hägg iron carbide (Fe_5C_2) has a monoclinic unit cell (a = 11.5620 Å, b = 4.5727 Å, c = 5.0595 Å, and β = 97.74°).[53] The optimized unit cell parameters are a = 11.5007 Å, b = 4.4789 Å, c = 4.9536 Å, and β = 97.63° (Figure 1). We optionally chose the (001), (100), and (110) surfaces for our model computations (Figure 2). For comparison, the three bare surfaces were optimized. The energetic differences between the bare and optimized surfaces of (001), (110), and (100) were 1.96, 1.78, and 0.44 eV, respectively. The differences in the averaged Fe−C and Fe−Fe distances between the bare and optimized surfaces were 0.147 and 0.107, 0.044 and 0.083, and 0.032 and 0.042 Å, respectively**.** These small energetic and geometric differences reveal the quality of the employed theoretical methods.

The Fe_5C_2(001) surface was modeled by a slab of three-layered carbon and five-layered iron atoms with a p(1×1) surface unit cell, as shown in Figure 2a. In the calculations, the bottom two-layered carbon and two-layered iron atoms were

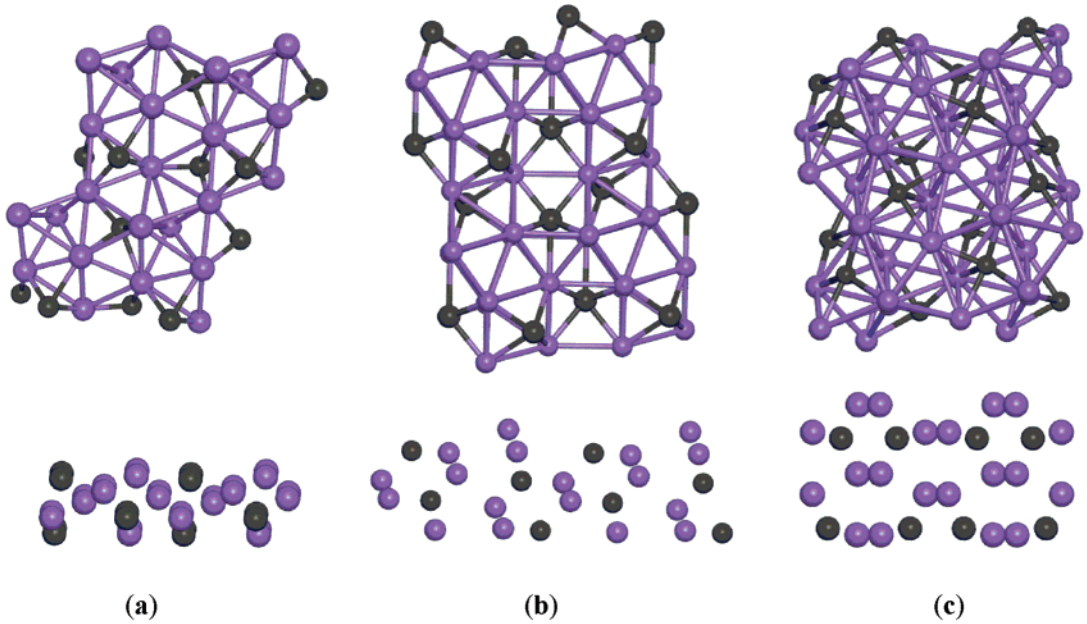

Figure 2. Schematic top and front views of Fe_5C_2(001) (a), top and side views of (110) (b), and top and front views of (100) (c) in a p(2×2) unit cell.

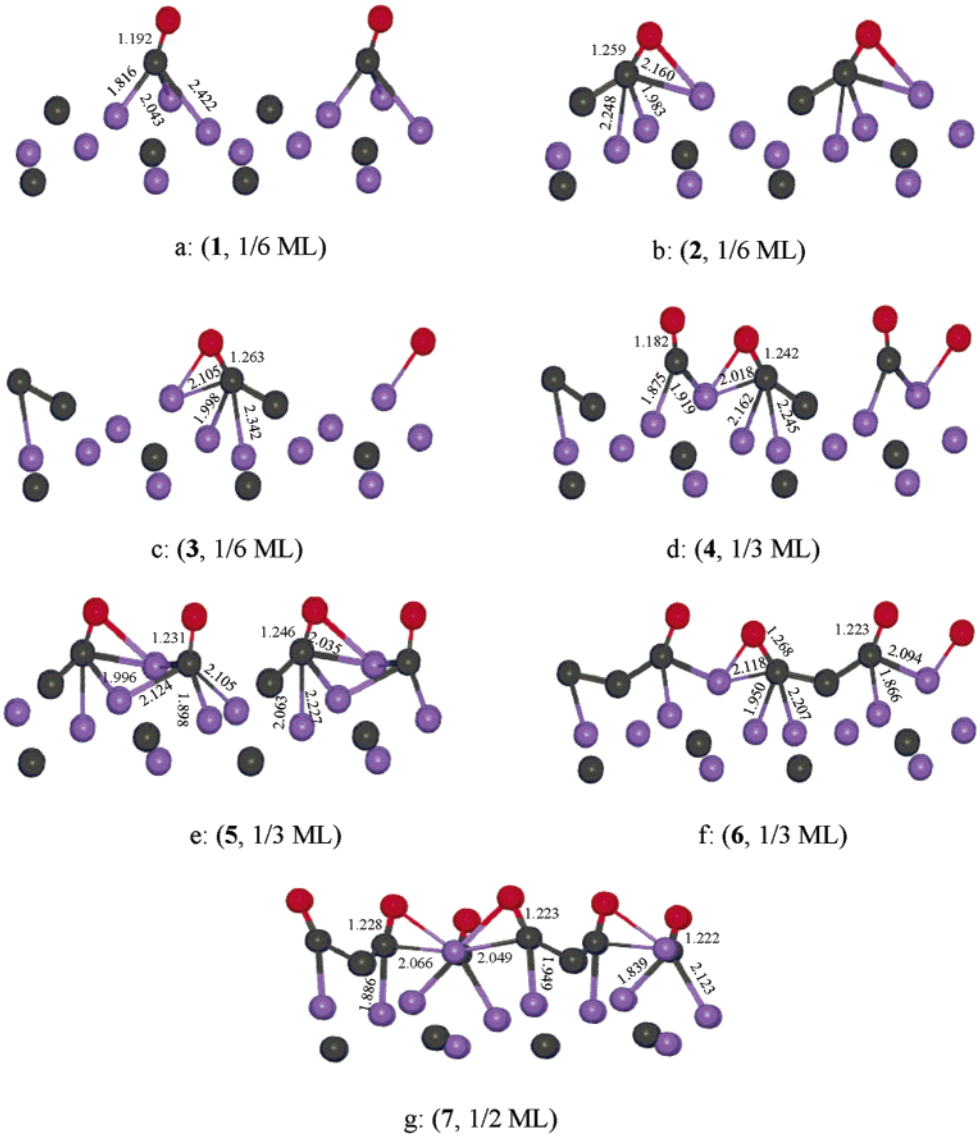

Figure 3. Schematic front views of CO adsorption on Fe_5C_2(001) (purple, Fe atom; gray, C atom; red, O atom).

fixed in their bulk positions, while the top three-layered iron and one-layered carbon atoms were allowed to relax. A $3 \times 5 \times 2$ *k* grid sampling within the Brillouin zones was used in the p(1×1) unit cell. We tested the *k* point sampling by using the $4 \times 6 \times 2$ Monkhorst−Pack meshes for the unit cell and found the error of the calculated energies to be less than 0.02 eV. For checking the influence of the thickness, we also performed calculations on a model system with three-layered carbon and seven-layered iron atoms under the relaxation of the top two-layered carbon and four-layered iron atoms, and the adsorption energy of species **1** and **2** (see the Results) decreases by 0.04 and 0.19 eV, respectively.

For the Fe_5C_2(110) surface, a slab consisting of six-layered iron and four-layered carbon atoms with a p(1×1) surface unit cell was modeled (Figure 2b). In the calculations, the bottom three-layered iron and two-layered carbon atoms were fixed in their bulk positions, while the top three-layered iron and two-layered carbon atoms were allowed to relax. A *k* point sampling was performed using $4 \times 3 \times 1$ Monkhorst−Pack meshes for the unit cell. Comparison with the energy of the $5 \times 4 \times 2$ Monkhorst−Pack meshes for the unit cell shows that the error is less than 0.02 eV. It is found that a slab of five-layered iron and three-layered carbon atoms under the relaxation of the top three-layered iron and two-layered carbon atoms results in energy changes in species **8** and **11** (see the Results) of only 0.07 and −0.09 eV. A test calculation on a slab of six-layered iron and four-layered carbon atoms under the relaxation of the top four-layered iron and three-layered carbon atoms results in energy changes of only −0.01 and 0.04 eV, respectively.

For the Fe_5C_2(100) surface, a slab composed of five-layered iron and two-layered carbon atoms with a p(1×1) surface unit cell was modeled (Figure 2c). In the calculations, the bottom two-layered iron and one-layered carbon atoms were fixed in their bulk positions, while the top three-layered iron and one-layered carbon atoms were allowed to relax. A *k* point sampling of the $4 \times 4 \times 1$ Monkhorst−Pack meshes for the unit cell was used. Comparison with the energy using the $5 \times 5 \times 2$ Monkhorst−Pack meshes for the unit cell shows that the error was less than 0.02 eV. With a slab of four-layered iron and one-layered carbon atoms under the relaxation of the top two-layered iron and one-layered carbon atoms, the changes in adsorption energy in species **15** and **18** (See the Results) are 0.02 and 0.05 eV. Thus, there is no significant effect of the slab thickness in both relaxed and fixed layers on the adsorption energy in all surfaces.

All initial orientations, such as the top, 2-fold, 3-fold, and 4-fold sites on the three surfaces, were considered, and the initial Fe−CO distances in the range of 1.8−2.2 Å were taken from

TABLE 1: Adsorption Energies per Molecule (eV) and Selected Bond Lengths (Å) for Various Coverages (ML) of CO on Fe_5C_2(001)

	1, 1/6 ML	**2**, 1/6 ML	**3**, 1/6 ML	**4**, 1/3 ML	**5**, 1/3 ML	**6**, 1/3 ML	**7**, 1/2 ML
E_{ads}	−2.10	−2.10	−2.08	−1.96	−1.92	−1.74	−1.25
d_{C-O}	1.192	1.259	1.263	1.182	1.231	1.223	1.223
				1.242	1.246	1.268	1.228
							1.222
d_{C-Fe}	1.816	1.983	1.998	1.875	1.898	1.866	1.949
	2.043	2.160	2.105	1.919	1.996	2.094	2.049
	2.422	2.248	2.342	2.018	2.105	1.950	1.886
				2.162	2.124	2.118	2.066
				2.245	2.035	2.207	1.839
					2.063		1.886
					2.227		2.123
d_{O-Fe}		2.104	2.035	2.061	2.116	2.345	2.127
						2.002	2.155
							2.115
d_{C-C}		1.374	1.370	1.352	1.365	1.439	1.425
						1.399	1.424
θ^a (deg)	87	69	68	72, 71	85, 65	78, 79	84, 64, 50

[a] Angle between the CO axis and *y* axis.

the available literature data of the related structures. However, optimization from all initial positions of CO adsorption converges to the same minimum-energy structure, and therefore, this minimum structure can also be considered as the most stable structure. The adsorption energy per CO molecule was defined as $E_{ads} = E(CO/slab) - (E(CO) + E(slab))$, where the first term is the total energy for the slabs with adsorbed species on the surface, the second term is the total energy of free CO, and the third term is the total energy of the bare slab of the surface. Therefore, the more negative the E_{ads}, the higher the adsorption energy.

Results and Discussion

(A) CO Adsorption on Fe_5C_2(001). For the bare Fe_5C_2(001) surface, CO deposits on the surface defects. As shown in Figure 3, there are three forms (**1**−**3**) of CO adsorption on Fe_5C_2(001) at 1/6 ML, and the computed bond parameters are listed in Table 1 and in Figure 3. In **1**, CO is in an apical capping adsorption mode, and the coordinating carbon stands over a triangular face of three iron atoms (Figure 3a). The adsorption energy is −2.10 eV. The C−O bond length is 1.192 Å, longer than the computed (1.144 Å) and measured (1.128 Å) values of free CO, implying an activation of CO in this mode. The angle between the CO and *y* axes is 87°. In **2** and **3**, CO is adsorbed at the 4-fold site (three iron atoms and one surface carbon atom, Figure 3b,c). The adsorption energies are −2.10 and −2.08 eV, respectively. The C−O bond lengths and the corresponding angles between the CO and *y* axes are 1.259 and 1.263 Å and 69° and 68°, respectively. Similarly, the C−O bond length is 1.30 Å, when CO is adsorbed on the 4-fold site on Fe(001).[47] The angle between the CO axis and the normal to the surface is 54°.[47] The tilted position of CO enables oxygen atoms to directly bond with the iron atoms. In addition, the distances of the CO carbon and the surface carbon in **2** and **3** are 1.374 and 1.370 Å, respectively, indicating the formation of new C−C bonds. The $C_{surface}$−CO bonds are very important and necessary for the exchange of carbon and the C−C coupling on the surfaces in FTS, since Stockwell et al.[54] verified with ^{13}C traces that surface carbons of carbide catalysts are incorporated into the FTS products.

To examine the impact of the surface coverage, we investigate the bonding patterns at 1/3 ML. There are three CO adsorption forms (**4**−**6**), and the computed bond parameters are given in Table 1. In **4** (Figure 3d), CO adsorption is at the 2-fold and 4-fold sites, and the corresponding adsorption energy is −1.96 eV. The oxygen and carbon atoms of the CO on the 4-fold site and the carbon atom in CO on the 2-fold site share one iron atom. The C−O bond lengths at the 2-fold and 4-fold sites are 1.182 and 1.242 Å, respectively. In **5** (Figure 3e), CO is adsorbed at two 4-fold sites, and the adsorption energy is −1.92 eV. The carbon and oxygen atoms at one of the 4-fold sites and the carbon atom at the other 4-fold site share two iron atoms. The bond parameters of **5** are similar to those of **4**. The C−O bond lengths are 1.231 and 1.246 Å, respectively. In **6** (Figure 3f), CO is also adsorbed at two 4-fold sites as in **5**, and the adsorption energy is −1.74 eV, which is lower than those of **4** and **5** by 0.22 and 0.18 eV, respectively. Two carbon atoms adsorbed on the two 4-fold sites share one carbon atom of Fe_5C_2-(001) with the formation of two C−C bonds in **6**. The related C−O bond lengths of the adsorbed CO on the two 4-fold sites are 1.223 and 1.268 Å.

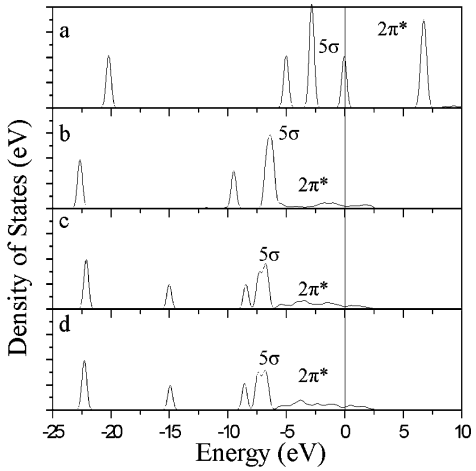

Figure 4. LDOS of the σ and π^* orbitals of free (a) and adsorbed (b, **1**; c, **2**; d, **3**) CO on Fe_5C_2(001) at 1/6 ML.

The Fe_5C_2(001) surface adsorbing CO at 1/2 ML (**7**) is shown in Figure 3g. The adsorption energy is −1.25 eV due to the stronger repulsion between the CO species on the surface as compared to that of **1** at 1/6 ML. The computed bond parameters are listed in Table 1. The C−O bond lengths of both 4-fold sites are 1.223 and 1.228 Å, respectively. The very tilted CO on the 3-fold site increases the C−O bond length to 1.222 Å. The tilted CO at the three sites leads to the formation of Fe−O bonds. The C−O bonds are all elongated, and strongly weakened at high coverage.

To analyze the electronic structure of Fe_5C_2(001) adsorbing CO, we examine the LDOS of the σ and π orbitals of the adsorbed CO. As shown in Figure 4a, the occupied 5σ orbital of free CO is at the Fermi level, while the bands of the adsorbed CO in **1**−**3** (Figure 4b−d) shift downward. The primary shifting of the 5σ and 2π^* bands is the result of the 5σ−d forward donation and d−2π^* back-donation.[29] The 5σ bands shift downward to the energy levels of −6.4, −6.8, and −6.8 eV for **1**−**3**, respectively. The intensity of the 5σ band in **1** (5.9 eV, Figure 4b) is higher than those in **2** and **3** (3.6 and 3.1 eV, Figure 4c,d), indicating the electron donation from the adsorbed CO in **1** to surface iron atoms (d orbitals) is stronger than in **2** and **3**. Similarly, the 5σ donation is important for CO adsorption on TiC,[55] TiO_2,[56] and ZnO.[57] The split of the 5σ bands in **2** and **3** is due to the formation of the new Fe−C and C−C bonds, in line with CO adsorption on the 4-fold sites of **2** and **3**.

As shown in Figure 4a, the unoccupied 2π^* orbital of free CO is higher than the Fermi level by 6.8 eV. In **1**−**3** (Figure

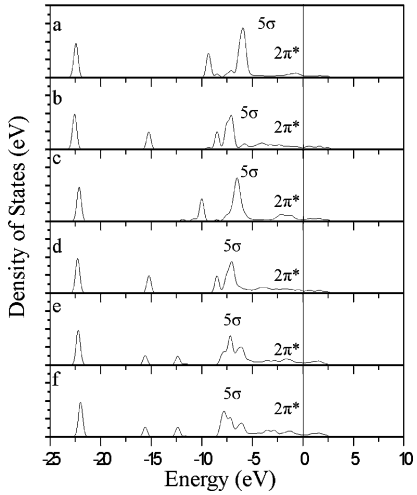

Figure 5. LDOS of the σ and π^* orbitals of adsorbed CO (a, b, **4**; c, d, **5**; e, f, **6**) on Fe_5C_2(001) at 1/3 ML.

4b−d), the $2\pi^*$ bands are broadened and shifted downward to −1.7, −3.5, and −3.8 eV levels, respectively, because of the back-donation of the iron d orbitals. The $2\pi^*$ intensities in **2** and **3** (0.7 and 0.8 eV) are higher than that in **1** (0.4 eV). This indicates a greater back-donation from the iron d orbitals into the CO $2\pi^*$ antibonding orbitals in **2** and **3** than that in **1**. $2\pi^*$ lies quite below the Fermi level, which indicates a very large charge transfer to CO. Mulliken population analysis[58−60] shows the electron population of the C 2p orbital of CO is 1.90 e. The electron populations of the C 2p orbitals of CO in **1**−**3** are 2.77, 2.94, and 2.91 e, respectively. Much of the electron charge of the surrounding Fe atoms goes into the $2\pi^*$ orbital of CO, which leads to the weakening of the C−O bonds.[61] There is a larger charge transfer to CO in **2** and **3** than that in **1**. As a result, the C−O bonds in **2** and **3** are strongly weakened. It has been observed that the C−O bond is strongly weakened due to the strong d−$2\pi^*$ back-donation when CO is adsorbed at the 4-fold site on Fe(100).[62−64]

As in **1**−**3**, the 5σ bands of CO species on the 2-fold and 4-fold sites in **4** also shift downward to −6.0 and −7.1 eV levels (Figure 5a,b), and the corresponding 5σ intensities in **4** are 5.5 and 3.8 eV. The 5σ bands of the CO species on the two 4-fold sites in **5** shift downward to −6.5 and −7.0 eV (Figure 5c,d), and the corresponding 5σ intensities in **5** are 4.8 and 3.5 eV. The 5σ bands of the CO species on the two 4-fold sites in **6** shift downward to −7.2 and −7.8 eV (Figure 5e,f), and the corresponding 5σ intensities in **6** are 3.2 and 2.9 eV. This implies that the lateral interaction between the CO molecules increases from **4** to **6** as the adsorption energy decreases from **4** to **6**. Furthermore, differently from **4** and **5**, two new $C_{surface}$−C bonds on two 4-fold sites are formed in **6**. In addition, CO adsorption is very hindered around the surface carbon atoms. The corresponding $2\pi^*$ intensities are 0.3 and. 0.7 eV in **4**, 0.7 and 0.6 eV in **5**, and 0.7 and 0.7 eV in **6** (Figure 5). Compared with species **1**−**3** at 1/6 ML, there is little difference in the $2\pi^*$ intensities in **4**−**6** at 1/6 ML. As in **1**−**3**, the corresponding electron populations of the C 2p orbitals of CO are 2.69 and. 2.94 e in **4**, 2.90 and 2.96 e in **5**, and 2.87 and 2.91 e in **6**. There is a similarity of a large charge transfer to CO between **1**−**3** and **4**−**6**.

The LDOS of the 5σ and $2\pi^*$ orbitals of adsorbed CO is shown in Figure 6. The 5σ bands of the CO species on two 4-fold sites and one 3-fold site in **7** shift downward to −7.4, −7.4, and −7.1 eV (Figure 6), and the corresponding 5σ intensities in **7** are 2.2, 2.7, and 1.8 eV, which are lower than

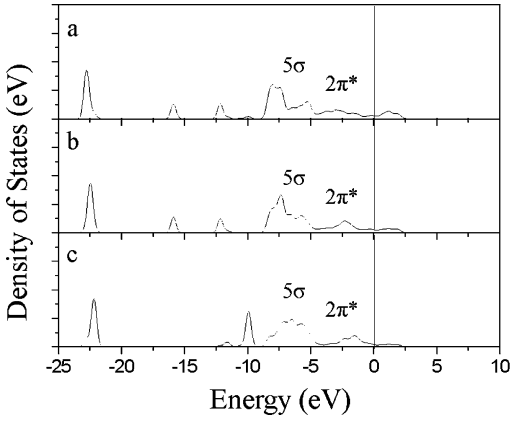

Figure 6. LDOS of the σ and π^* orbitals of adsorbed CO (**7**) on Fe_5C_2-(001) at 1/2 ML.

in **1**−**6**. This indicates strong lateral interaction between adsorbed CO molecules. The corresponding $2\pi^*$ intensities in **7** are about 0.8, 0.8, and 0.6 eV (Figure 6). The electron populations of the C 2p orbitals of CO in **7** are 2.80, 2.83, and 2.85 e. The large charge transfer to CO leads to weakening of the C−O bonds.

(B) CO Adsorption on Fe_5C_2(110). The four optimized forms (**8**−**11**) of CO adsorption on Fe_5C_2(110) at 1/6 ML are shown in Figure 7, and the bond parameters are summarized in Table 2 and in Figure 7. CO prefers to adsorb around iron atoms. The adsorption energies of the 3-fold and 4-fold sites (**8**, **9**, Figure 7a,b) are −2.34 and −2.23 eV, respectively. The activated C−O bond length in **9** is 1.254 Å and is longer than that in **8** by 1.199 Å. The angle between the CO and *z* axis in **9** is 57° and is smaller than that in **8** by 73°. The other two modes (**10**, **11**, Figure 7c,d) have CO adsorbed around surface carbon atoms. The $C_{surface}$−C bond lengths are 1.407 and 1.373 Å. The adsorption energies in **10** and **11** are −1.65 and −1.16 eV. The C−O bond lengths are 1.284 and 1.201 Å, respectively.

We also examine the CO adsorption modes at 1/3 ML. There are three optimized patterns (**12**−**14**, Figure 7e−g) with adsorption energies of −2.10, −1.88, and −1.80 eV. The bond parameters of **12**−**14** are given in Table 2. In **12**, CO is only bonded with iron atoms at a 3-fold site and a top site. The corresponding activated C−O bond lengths are 1.184 and 1.168 Å. In **13** and **14**, CO adsorbs at a 3-fold site and a 4-fold site. CO is bonded to the surface carbon atoms of 4-fold sites with elongated C−O bond lengths of 1.192 vs 1.277 and 1.194 vs 1.261 Å in **13** and **14**, respectively.

The 5σ bands of the adsorbed CO in **8**−**11** shift downward to −6.2, −6.7, −7.0, and −6.8 eV (Figure 8), and the corresponding 5σ intensities of the adsorbed CO species are 5.6, 4.3, 3.5, and 5.9 eV, respectively. The 5σ orbitals of CO in **10** and **11** are split due to the formation of the $C_{surface}$−C bonds. On the other hand, the $2\pi^*$ bands of the CO species in **8**−**11** shift downward to −1.3, −1.3, −3.0, and −0.9 eV, and the corresponding $2\pi^*$ intensities are 0.6, 0.7, 0.6, and 0.5 eV (Figure 8). The $2\pi^*$ intensities in **10** and **11** are a little lower than those in **2** and **3**, 0.7 and 0.8 eV, on Fe_5C_2(001), and the adsorption energies of the former are lower than those of the latter. There is a large charge transfer from surrounding Fe atoms to CO in **8**−**11**. The electron populations of the C 2p orbitals of CO in **8**−**11** are 2.84, 2.87, 3.00, and 2.82 e, respectively. Among them, the largest charge transfer to CO in **10** is in line with the longest C−O bond lengths.

The LDOS shows 5σ bands of CO species on the 3-fold and top sites in **12** shift downward to −6.6 and −6.1 eV levels

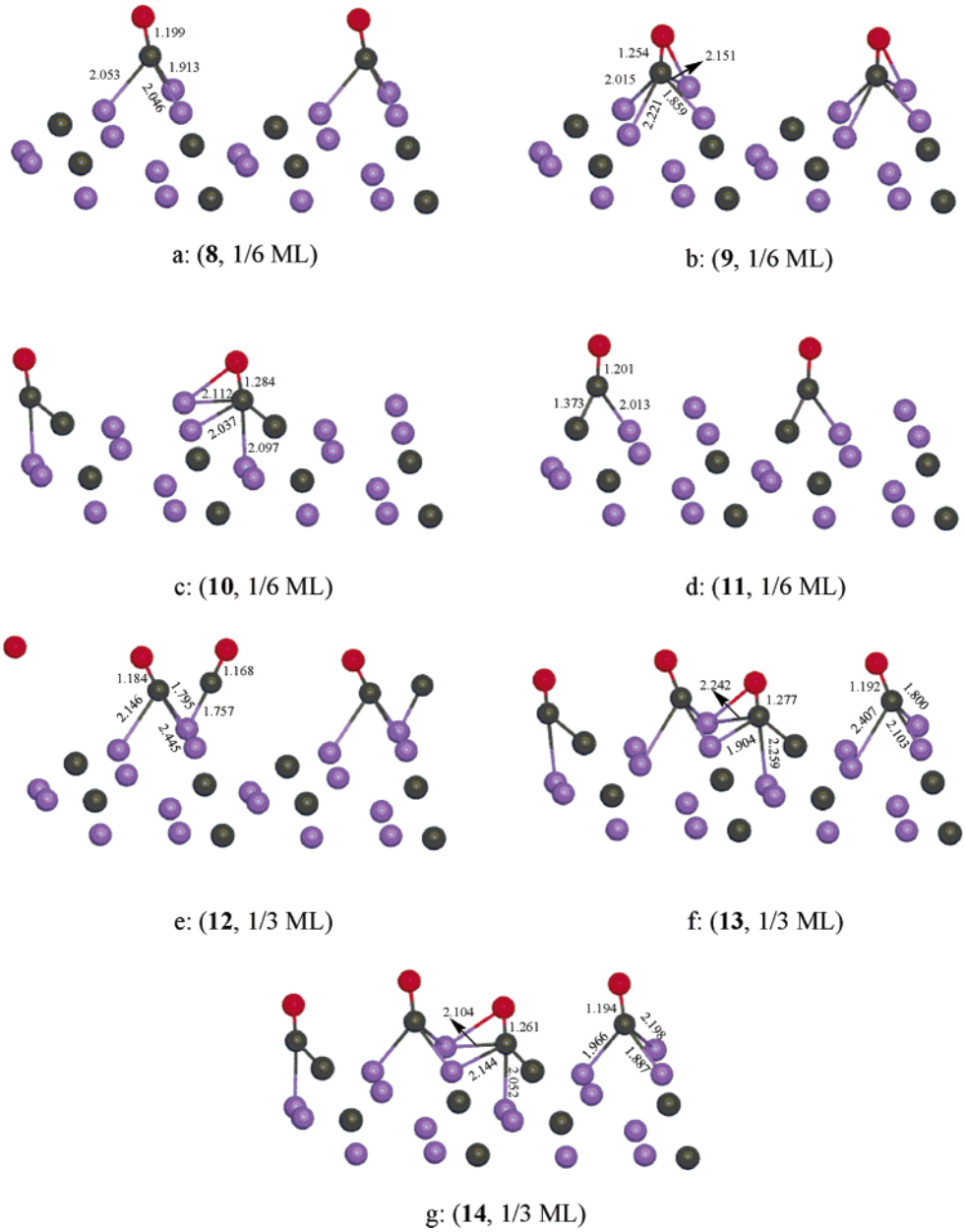

Figure 7. Schematic side views of CO adsorption on Fe_5C_2(110).

TABLE 2: Adsorption Energies per Molecule (eV) and Selected Bond Lengths (Å) for Various Coverages (ML) of CO on Fe_5C_2(110)

	8, 1/6 ML	**9**, 1/6 ML	**10**, 1/6 ML	**11**, 1/6 ML	**12**, 1/3 ML	**13**, 1/3 ML	**14**, 1/3 ML
E_{ads}	−2.34	−2.23	−1.65	−1.16	−2.10	−1.88	−1.80
d_{C-O}	1.199	1.254	1.284	1.201	1.184	1.192	1.194
					1.168	1.277	1.261
d_{C-Fe}	1.913	1.859	2.037	2.013	1.795	1.800	1.887
	2.046	2.015	2.097		2.146	2.103	1.966
	2.053	2.151	2.112		2.445	2.407	2.198
		2.221			1.757	1.904	2.052
						2.242	2.104
						2.259	2.144
d_{O-Fe}		2.083	2.013			2.020	2.106
d_{C-C}			1.407	1.373		1.435	1.404
θ^a (deg)	73	57	59	80	66, 66	83, 51	88, 57

[a] Angle between the CO axis and *z* axis.

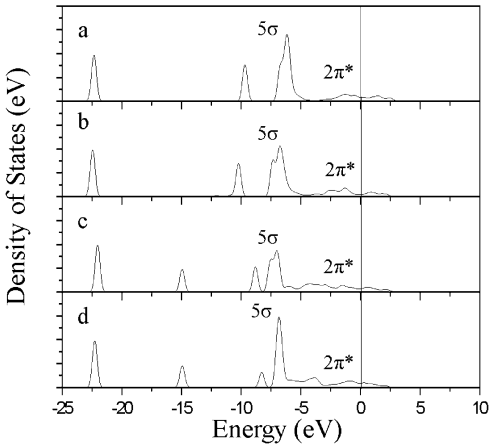

Figure 8. LDOS of the σ and π^* orbitals of adsorbed CO (a, **8**; b, **9**; c, **10**; d, **11**) on Fe_5C_2(110) at 1/6 ML.

(Figure 9a,b), respectively, and the corresponding 5σ intensities are 4.5 and 4.1 eV. The 5σ bands of the 3-fold and 4-fold sites in **13** shift downward to −6.4 and −6.8 eV (Figure 9c,d), respectively, and the corresponding 5σ intensities are 4.5 and 3.2 eV. The 5σ bands of the 3-fold and 4-fold sites in **14** shift

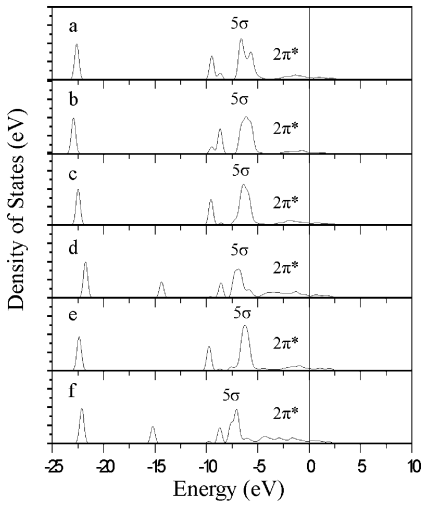

Figure 9. LDOS of the σ and π^* orbitals of adsorbed CO (a, b, **12**; c, d, **13**; e, f, **14**) on $Fe_5C_2(110)$ at 1/3 ML.

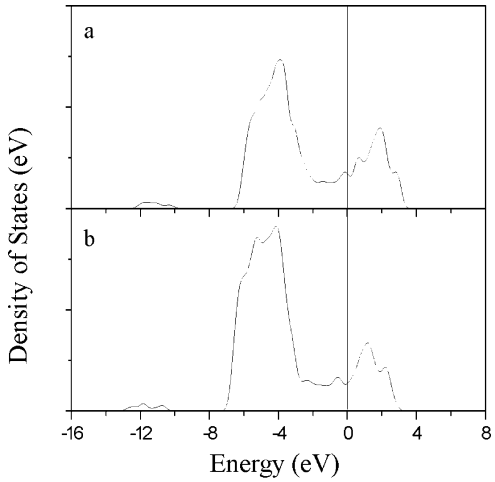

Figure 10. LDOS of the surface Fe−C bonds on $Fe_5C_2(001)$ (a) and $Fe_5C_2(110)$ (b).

downward to −6.3 and −7.0 eV (Figure 9e,f), respectively, and the corresponding 5σ intensities are 5.0 and 3.8 eV. The 5σ intensity in **12**−**14** at 1/3 ML is lower than that in **8**−**10** at 1/6 ML due to lateral interaction between CO molecules. In addition, the corresponding 2π^* intensities are 0.5 vs 0.4 eV in **12**, 0.5 vs 0.7 eV in **13,** and 0.6 vs 0.6 in **14** (Figure 9). The corresponding electron populations of the C 2p orbitals of CO are 2.73 vs 2.53 e in **12**, 2.88 vs 2.78 e in **13**, and 3.00 vs 2.81 e in **14**. The larger charge transfer to CO in **13** and **14** than that in **12** leads to longer activated C−O bond lengths in **13** and **14** than that in **12**.

At this step, the similarity between the (001) and (110) slabs is that the ML contains carbon atoms. The LDOS of surface carbon atoms is shown in Figure 10. The C 2p−Fe 3d hybridization of the C−Fe bonds of $Fe_5C_2(001)$ spans mainly from −6.9 to −1.0 eV (Figure 10a), while that of $Fe_5C_2(110)$ is in the range of −7.5 to −2.8 eV (Figure 10b). The intensities of the 2p−3d bands are 2.9 and 3.6 eV, respectively. This indicates stronger surface Fe−C bonds on $Fe_5C_2(110)$, which in turn hinders local CO adsorption. As a consequence, the CO adsorption energy of the species absorbed around the surface carbon atoms on (110) at 1/6 ML is lower than that on (001) by up to 0.94 eV.

(C) CO Adsorption on $Fe_5C_2(100)$. For the bare $Fe_5C_2(100)$ surface, the ML is only composed of iron atoms. There are two

TABLE 3: Adsorption Energies per Molecule (eV) and Selected Bond Lengths (Å) for Various Coverages (ML) of CO on $Fe_5C_2(100)$

	15, 1/4 ML	**16**, 1/4 ML	**17**, 1/4 ML	**18**, 1/4 ML	**19**, 1/2 ML	**20**, 1/2 ML
E_{ads}	−2.21	−2.21	−2.20	−2.20	−2.28	−1.89
d_{C-O}	1.200	1.200	1.169	1.170	1.182	1.160
					1.180	1.160
d_{C-Fe}	1.906	1.894	1.771	1.770	1.813	1.806
	1.940	1.960			2.054	1.802
	2.167	2.150			2.557	
					1.785	
					2.226	
					2.462	
θ^a (deg)	68	68	89	89	62, 67	70, 70

[a] Angle between the CO axis and *y* axis.

3-fold adsorbed forms (**15**, **16**) and two top ones (**17**, **18**) of CO adsorption on $Fe_5C_2(100)$ at 1/4 ML (Figure 11), and the computed bond parameters are summarized in Table 3. The adsorption energies of **15**−**18** are very close (−2.21 eV for **15** and **16** and −2.20 eV for **17** and **18**). The adsorption energy of the stable minimum on $Fe_5C_2(100)$ is similar to that on Fe_5C_2-(001) and -(110) at low coverage. The C−O bond lengths in **15** and **16** are both 1.200 Å (Figure 11a,b). The Fe−C bond lengths of **16** are similar to those of **15**. There are similar structural properties in **17** and **18**; e.g., the C−O bond lengths are 1.169 and 1.170 Å, respectively (Figure 11c,d).

There are two adsorption forms (**19** and **20**) when coverage becomes 1/2 ML (Figure 11e,f), and the bond parameters are shown in Table 3. In **19**, CO adsorbs at the two 3-fold sites, and the adsorption energy is −2.28 eV, which is even higher than the adsorption energy at lower coverage. The adsorption energy of a stable minimum at higher coverage on (100) is higher than that of **4** on (001) and **12** on (110). The C−O bond lengths are 1.182 and 1.180 Å. In **20**, CO adsorbs at the two top sites. The adsorption energy in **20** is −1.89 eV, lower than in **19**. Both C−O bonds are weakly activated by 1.160 Å.

We computed the LDOS for **15**−**18**. The 5σ bands of the adsorbed CO in **15**−**18** shift downward to about −6.0, −6.0, −5.9, and −5.9 eV (Figure 12), and the 5σ intensities of the adsorbed CO species in **15**−**18** are 5.0, 5.0, 8.0, and 7.9 eV, respectively. The 2π^* bands of CO in **15**−**18** shift downward to about −1.5, −1.5, −1.0, and −0.9 eV. The intensities of the 2π^* orbitals of the adsorbed CO in **15**−**18** are about 0.6, 06, 0.5, and 0.5 eV, respectively. The electron populations of the C 2p orbitals of CO in **15**−**18** are all 3.06 e. Compared with the electron population of the C 2p orbital of free CO, there is a large charge transfer from the surrounding Fe atoms to CO.

As in the cases of **15**−**18**, the 5σ bands of the CO species on the two 3-fold sites in **19** also shift downward to −6.4 and −5.7 eV (Figure 13a,b), respectively, and the corresponding 5σ intensities in **19** are 3.6 and 3.5 eV. The 5σ bands of both top sites in **20** shift downward to −6.0 eV (Figure 13c,d), respectively, and the corresponding 5σ intensities in **20** are 4.0 and 4.1 eV. The decrease of the 5σ intensity from **15** and **16** to **19** is about 1.4 eV, while that from **17** and **18** to **20** is about 4.0 eV. This implies that lateral interaction in **20** is stronger than that in **19**. In addition, the corresponding 2π^* intensities are 0.5 vs 0.4 eV in **19** and 0.4 vs 0.4 eV in **20** (Figure 13). The electron populations of the C 2p orbtitals of CO in **19** and **20** are 3.06 vs 3.06 e and 3.05 vs 3.06 e, respectively. There is little difference in charge transfer between **15**−**18** and **19** and **20**.

Our present DFT calculations have outlined an informative picture for CO adsorption on the three Fe_5C_2 surfaces. It is well-

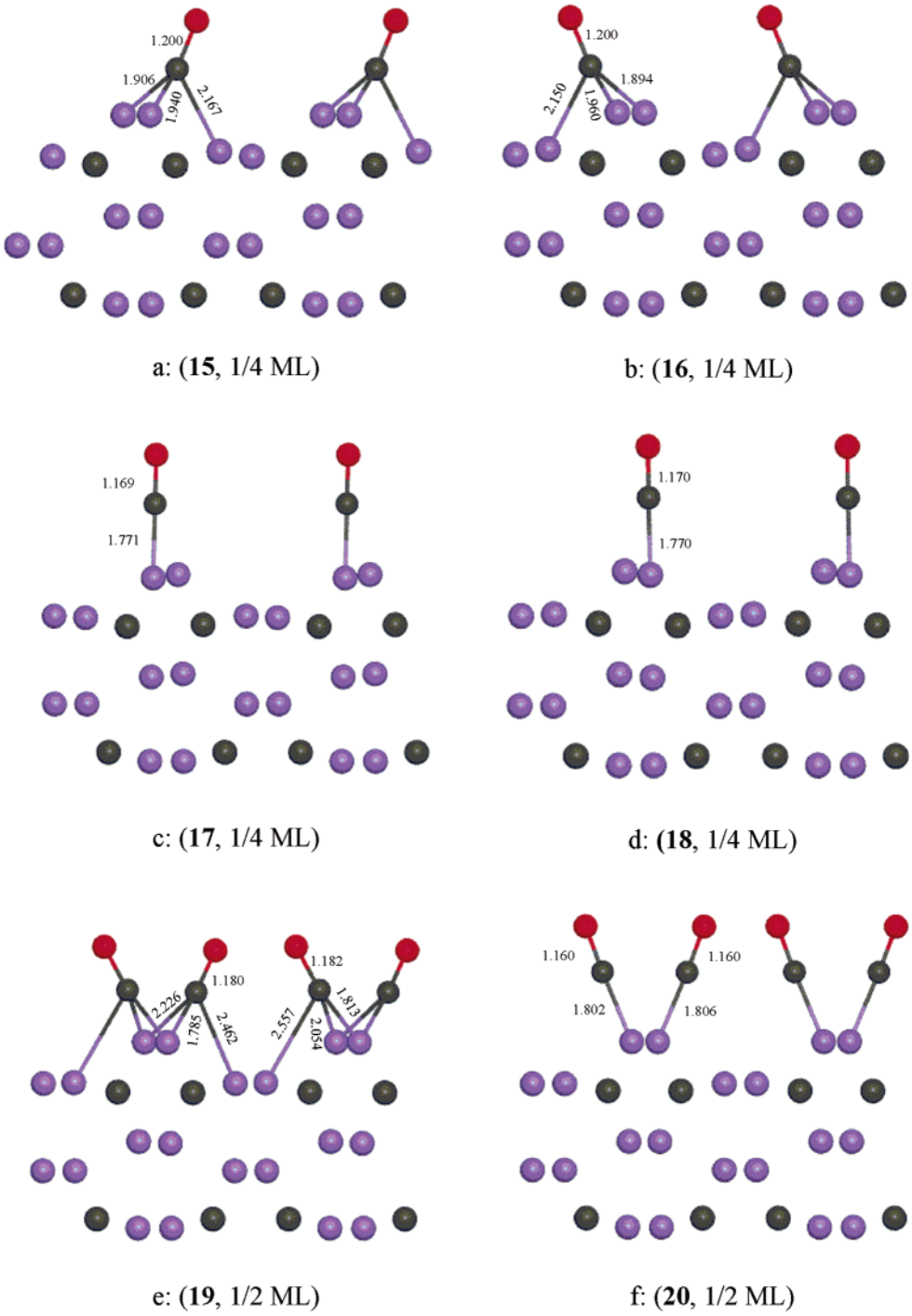

Figure 11. Schematic front views of CO adsorption on Fe_5C_2(100).

known that several types of carbide phases exist on a working iron-based FTS catalyst. The sites possibly active and carried by these phases may be even more complex. The experimental observations have pointed out that, among all these carbides, the Fe_5C_2 phase is the most distinguishing one for FTS catalysis. Understanding the activation mechanism of the main reactants (CO and H_2) on the surfaces of this phase is thus important to determine a way to explore the FTS mechanism on a more precise basis. Our study shows, for the first time, that, even on a regular crystal structure approximated by unit cell combinations, the phase may present three surfaces, i.e., (001), (110), and (100). Over these surfaces, the sites may be combined with many possibilities with regard only to CO adsorption.

Nevertheless, in the very beginning stage, CO adsorption on the most representative carbide phase can provide a picture for considering the FTS mechanism in a comprehensive way. It has been shown that the donation and back-donation between adsorbing CO molecule orbitals and the surface iron orbitals are essential in CO activation. On one hand, the electrons in the HOMO of a CO molecule are donated to the LUMO of the surface iron atoms, while in turn, the d electrons in the HOMO contributed by the surface iron atoms are donated back to the LUMO (π antibonding orbital, $2\pi^*$) of the adsorbed CO species, resulting in weakening of the strong C−O bond in a free CO; namely, CO is activated. In more detail, our DFT results show the heterogeneous nature of the sites on the Fe_5C_2 phase in CO activation. To stress this point, the adsorption energies for different CO adsorption forms on the three surfaces (001), (110), and (100) at different degrees of coverage are shown in Figure 14.

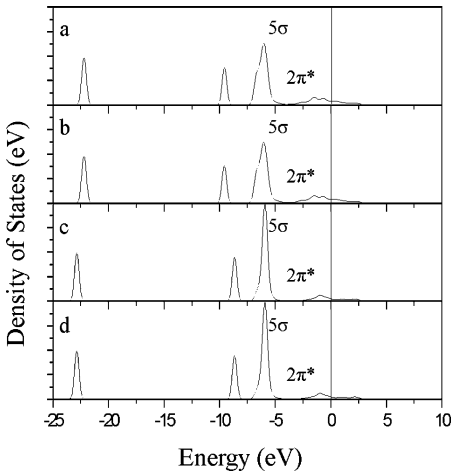

Figure 12. LDOS of the σ and π^* orbitals of adsorbed CO (a, **15**; b, **16**, c, **17**; d, **18**) on $Fe_5C_2(100)$ at 1/4 ML.

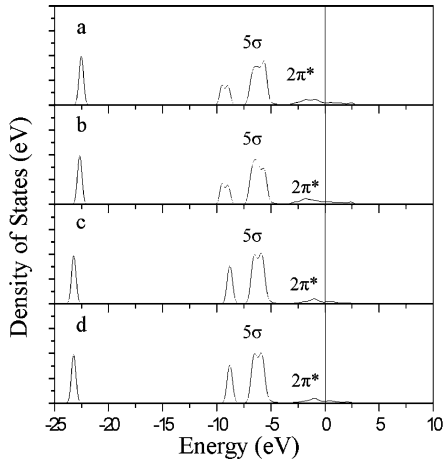

Figure 13. LDOS of the σ and π^* orbitals of adsorbed CO (a, b, **19**; c, d, **20**) on $Fe_5C_2(100)$ at 1/2 ML.

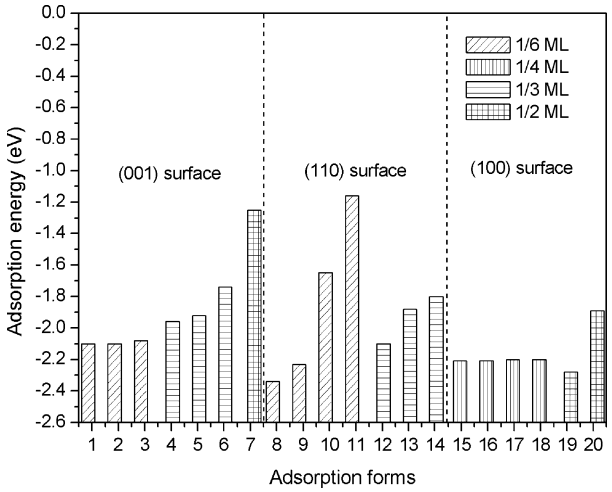

Figure 14. Adsorption energetics of CO adsorption on Fe_5C_2 surfaces.

From Figure 14, it can be seen that the (100) surface with adsorbed CO can reach the lowest energy level (the most negative adsorption energy) among the three surfaces with coverage up to 1/2 ML for the adsorption forms **15**−**19**. This implies that CO adsorption on the (100) surface is the most favorable adsorption case. It is surprising that, even at the highest coverage of 1/2 ML calculated here, an adsorption mode (**19**) exists with higher adsorption energy than all the other modes

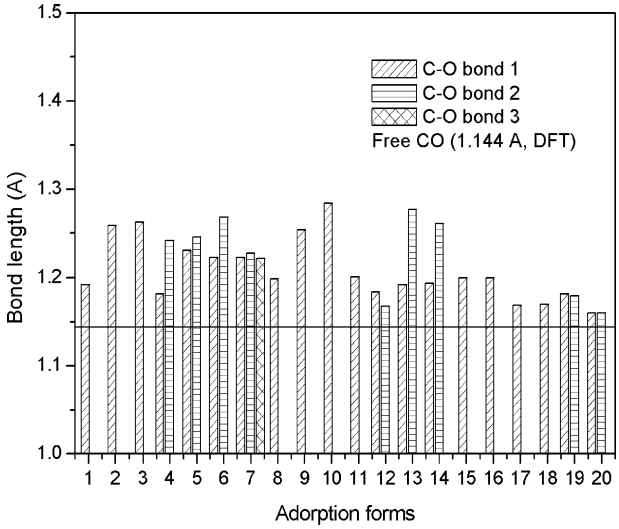

Figure 15. C−O bond activation for the 20 adsorption forms.

on all three surfaces. For the (110) surface, CO is favored to adsorb around iron atoms. Except adsorption modes **10** and **11**, all the other modes are comparable in energy level to those on (100). For comparison, the (100) surface should be first covered thermodynamically, and a competing adsorption on other surfaces can only occur after high coverage of the (100) surface is reached. No very low energy levels are found on (001) even at a low coverage (1/6 ML) compared to those found in (100) and (110).

However, the CO adsorption on (001) cannot be ruled out in FTS catalysis: (i) the energy levels with coverage below 1/2 ML are moderate compared to those on (110) and (001), (ii) in many cases, catalytic roles may be significantly suppressed if the reactant−surface interaction is too strong, i.e., moderate energetic levels might have a promoting effect for CO activation and FTS reactions, and (iii) practical FTS reactions on iron catalysts undergo a series of complex elementary steps, CO adsorption of which is the very beginning step, and the complexity of FTS indicates that the diverse activation forms may co-act in the FTS catalysis.

The C−O bond lengths in all adsorption modes are summarized in Figure 15. For all adsorption modes with low and moderate energy levels, the C−O bonds are all elongated, the longest C−O bond is found on (001) (**1**−**6**), and the shortest is on (100) (**15**−**20**) despite less favored adsorption on (001). The results provide the information that CO can be strongly activated on the (001) surface if energetically allowed, and moderately activated on (110) (**8**, **9**, **12**−**14**) and (100) (**15**−**20**). At this stage, the present DFT results reflect the complexity of CO activation on the selected catalyst phase. The diversity of the adsorption modes with different surface effects has come to be a sign for the FTS complexity. Nevertheless, further systematic investigation on the coadsorption of CO and H_2, carbon species hydrogenation, C−C coupling, and possible CO insertion into hydrocarbon species is expected to project helpful information for a better understanding of the FTS mechanism.

Conclusions

With the help of DFT calculations we investigated CO adsorption on the (001), (100) and (110) surfaces of Fe_5C_2, which are considered as active catalysts in Fischer−Tropsch synthesis. CO is adsorbed at the 3-fold (three iron atoms) and the 4-fold (three iron atoms and one carbon atom) sites on the $Fe_5C_2(001)$ surface at 1/6 ML, and the adsorption energy lies

in the narrow range of −2.08 to −2.10 eV. The 5σ donation at the 3-fold site is stronger than that at the 4-fold site, while the d−2π* back-donation at the latter is stronger than that at the former. Compared with the electron population of the C 2p orbital of the free CO, there is a large charge transfer from the surrounding Fe atoms to CO at the 4-fold site. This leads to the stronger C−O bond activation at the 4-fold site. For coverage at 1/3 ML, there are lateral interactions between the adsorbed CO molecules due to the decreased 5σ donation, while there is little difference in the d−2π* back-donation of the adsorption modes at 1/3 and 1/6 ML.

Furthermore, the adsorption energy becomes very low when CO is adsorbed at the two 4-fold sites sharing one surface carbon atom at 1/3 ML. This suggests that surface carbon atoms hinder local CO adsorption at higher coverage. For CO adsorption at 1/2 ML, there are strong lateral interactions among the adsorbed CO molecules, and this is the reason for the lower adsorption energy. The C−O bonds are very elongated, which is consistent with large charge transfer to CO.

For the Fe_5C_2(110) surface, we studied CO adsorption at 1/6 and 1/3 ML. CO prefers to adsorb around iron atoms at 1/6 ML, with −2.34 and −2.23 eV at 3-fold and 4-fold sites, respectively. The adsorption energy of CO adsorption around the surface carbon atoms is −1.65 and −1.16 eV at 1/6 ML. For comparison with the (001) surface, the CO adsorption energy of the species adsorbed around the surface carbon atoms on (110) at 1/6 ML is lower than that on (001) by up to 0.94 eV. This is due to the difference in surface electronic structure. The C 2p−Fe 3d bands mainly lie at lower energy on (110) than that on (001), indicating surface Fe−C bonds on (110) are stronger than those on (001), which hinders local CO adsorption. At high coverage, CO also prefers to adsorb around iron atoms by −2.10 eV.

In contrast, the (100) surface has only iron atoms, which form two 3-fold sites (three iron atoms) and two top sites at 1/4 ML. The adsorption energy at 1/4 ML lies in the small range of −2.20 to −2.21 eV. The adsorption energy on (100) at low coverage is similar to those on (001) and (110). Furthermore, CO favors adsorption on the 3-fold sites at 1/2 ML coverage on (100) with an adsorption energy of −2.28 eV. This is because lateral interactions on the 3-fold sites are weaker than those on the top sites. Compared with those on (001) and (110) at low coverage, the adsorption energy on (100) is similar. However, the adsorption energy on (100) at high coverage is higher than those on (001) and (110). As a consequence, CO adsorption is favored on Fe_5C_2(100).

These results indicate the diversity of the atomic structure on the underlying Fe_5C_2 surface site. Compared with the 2π* bands of the free CO, the 2π* bands in the 20 modes lie quite below the Fermi level. This indicates a very large charge transfer to CO. As a consequence, the C−O bonds are weakened. Although (100) at high coverage has the highest adsorption energy, other surfaces may play dominant roles when practical working conditions permit.

Acknowledgment. We thank the Key Project of the Chinese Academy of Sciences and the 863 Project of the Ministry of Science and Technology of China for financial support (Grants 2001AA523010 and KGC X1-SW-02).

References and Notes

(1) Anderson, R. B. *The Fischer−Tropsch Reaction*; Academic Press: London, U.K., 1984.

(2) Bian, G.; Oonuki, A.; Koizumi, N.; Nomoto, H.; Yamada, M. *J. Mol. Catal. A* **2002**, *186*, 203.

(3) Datye, A. K.; Jin, Y. M.; Mansker, L.; Motjope, R. T.; Dlamini, T. H.; Coville, N. J. *Stud. Surf. Sci. Catal.* **2000**, *130B*, 1139.

(4) Jin, Y. M.; Mansker, L.; Datye, A. K. *Prepr.—Am. Chem. Soc., Div. Pet. Chem.* **1999**, *44*, 97.

(5) Bartholomew, C. H.; Stoker, M. W.; Mansker, L. Datye, A. K. *Stud. Surf. Sci. Catal.* **1999**, *126*, 265.

(6) Zhang, Y. Q.; O'Brien, R. J.; Davis, B. H.; Hamdeh, H. H. *Prepr.—Am. Chem. Soc., Div. Pet. Chem.* **1999**, *44*, 100.

(7) Jin, Y. M.; Datye, A. K. *Stud. Surf. Sci. Catal.* **1998**, *119*, 209.

(8) Davis, B. H. *Catal. Today* **2003**, *84*, 83.

(9) O'Brien, R. J.; Xu, L. G.; Spicer, R. L.; Davis, B. H. *Energy Fuels* **1996**, *10*, 921.

(10) Rao, K. R. P. M.; Huggins, F. E.; Mahajan, V.; Huffman, G. P.; Burkur, D. B.; Rao, V. U. S. *Hyperfine Interact.* **1994**, *93*, 1751.

(11) Fournier, J.; Carreiro L.; Qian, Y. T.; Soled, S.; Kershaw, R.; Dwight, K.; Wold, A. *J. Solid State Chem.* **1985**, *58*, 211.

(12) Shroff, M. D.; Kalakkad, D. S.; Coulter, K. E.; Köhler, S. D.; Harrington, M. S.; Jackson, N. B.; Sault, A. G.; Datye, A. K. *J. Catal.* **1995**, *156*, 185.

(13) Amelse, J. A.; Schwartz, L. H.; Butt, J. B. *J. Catal.* **1981**, *72*, 95.

(14) Niemantsverdriet, J. W.; Van der Kraan, A. M. *J. Catal.* **1981**, *72*, 375.

(15) Niemantsverdriet, J. W.; Van der Kraan, A. M.; Van Dijk, W. L.; Van der Baan, H. S. *J. Phys. Chem.* **1980**, *84*, 3363.

(16) Kalakkad, D. S.; Shroff, M. D.; Köhler, S. D.; Jackson, N. B.; Datye, A. K. *Appl. Catal., A* **1995**, *133*, 335.

(17) Dictor, R. A.; Bell, A. T. *J. Catal.* **1986**, *97*, 121.

(18) Rao, K. R. P. M.; Huggins, F. E.; Mahajan, V.; Huffman, G. P.; Rao, V. U. S.; Bhatt, B. L.; Burkur, D. B.; Davis, B. H.; O'Brien, R. *J. Top. Catal.* **1995**, *2*, 71.

(19) Huang, C. S.; Xu, L.; Davis, B. H. *Fuel Sci. Technol. Int.* **1993**, *11*, 639.

(20) Loaiza-Gil, A.; Fontal, B.; Rueda, F.; Mendiadua, J.; Casanova, R. *Appl. Catal., A* **1999**, *177*, 193.

(21) Turner, M. L.; Marsih, N.; Mann, B. E.; Quyoum, R.; Long, H. C.; Maitlis, P. M. *J. Am. Chem. Soc.* **2002**, *124*, 10456.

(22) Overett, M. J.; Hill, R. O. Moss, J. R. *Coord. Chem. Rev.* **2000**, *206−207*, 581.

(23) Vannice, M. A. In *Catalysis Science and Technology*; Anderson, J. B., Boudart, M., Eds.; Springer-Verlag: Berlin, 1982; Vol. *3*.

(24) Eastman, D. E. *Solid State Commun.* **1972**, *10*, 933.

(25) Broden, G.; Gafner, G.; Bonzel, H. *Appl. Phys.* **1977**, *13*, 33.

(26) Jensen, E. S.; Rhodin, T. N. *Phys. Rev. B* **1983**, *27*, 3338.

(27) Greuter, F.; Heskett, D.; Plummer, E. W.; Freund, H. J. *Phys. Rev. B* **1983**, *27*, 7117.

(28) Engel, T.; Ertl, G. *Adv. Catal.* **1979**, *28*, 1.

(29) Sung, S. S.; Hoffmann, R. *J. Am. Chem. Soc.* **1985**, *107*, 578.

(30) Krause, S.; Mariani, C.; Pince, K. C.; Horn, K. *Surf. Sci.* **1984**, *138*, 305.

(31) Saiki, R. S.; Herman, G. S.; Yamada, M.; Osterwalder, J.; Fadley, C. S. *Phys. Rev. Lett.* **1989**, *63*, 283.

(32) Kiskinova, M.; Szab, A.; Yates, J. T., Jr. *Surf. Sci.* **1988**, *205*, 215.

(33) Wong, Y. T.; Hoffmann, R. *J. Phys. Chem.* **1991**, *95*, 859.

(34) Delbecq, F.; Moraweck, B.; Vérité, L. *Surf. Sci.* **1998**, *396*, 156.

(35) Delbecq, F.; Sautet, P. *Chem. Phys. Lett.* **1999**, *302*, 91.

(36) Delbecq, F.; Sautet, P. *Phys. Rev. B* **1999**, *59*, 5142.

(37) Ciobîcă, I. M.; Kleyn, A. W.; van Santen, R. A. *J. Phys. Chem. B* **2003**, *107*, 164.

(38) Liu, Z. P.; Hu, P. *J. Am. Chem. Soc.* **2003**, *125*, 1958.

(39) Karmazyn, A. D.; Fiorin, V.; Jenkins, S. J.; King, D. A. *Surf. Sci.* **2003**, *538*, 171.

(40) Shah, V.; Li, T.; Baumert, K. L.; Cheng, H. S.; Sholl, D. S. *Surf. Sci.* **2003**, *537*, 217.

(41) Hammer, B.; Nielsen, O. H.; Nørskov, J. K. *Catal. Lett.* **1997**, *46*, 31.

(42) White, J. A.; Bird, D. M. *Phys. Rev. B* **1994**, *50*, 4954.

(43) (a) Payne, M. C.; Allan, D. C.; Arias, T. A.; Joannopoulos, J. D. *Rev. Mod. Phys.* **1992**, *64*, 1045. (b) Milman, V.; Winkler, B.; White, J. A.; Pickard, C. J.; Payne, M. C.; Akhmataskaya, E. V.; Nobes, R. H. *Int. J. Quantum Chem.* **2000**, *77*, 895.

(44) Vanderbilt, D. *Phys. Rev. B* **1990**, *41*, 7892.

(45) Monkhorst, H. J.; Pack, J. D. *Phys. Rev. B* **1976**, *13*, 5188.

(46) Louie, S. G.; Froyen, S.; Cohen, M. L. *Phys. Rev. B* **1982**, *26*, 1738.

(47) Nayak, S. K.; Nooijen, M.; Bernasek, S. L. *J. Phys. Chem. B* **2001**, *105*, 164.

(48) Cheng, H. S.; Reiser, D. B.; Dean, S. W., Jr.; Baumert, K. *J. Phys. Chem. B* **2001**, *105*, 12547.

(49) Ge, Q.; Neurock, M.; Wright. H. A.; Srinivasan, N. *J. Phys. Chem. B* **2002**, *106*, 2826.

(50) Ge, Q.; Jenkins, S. J.; King, D. A. *Chem. Phys. Lett.* **2000**, *327*, 125.

(51) Le Caer, G.; Simon, A.; Lorenzo, A.; Genin, J. M. *Phys. Status Solidi A* **1971**, *6*, K97.
(52) Immel, S. *Molarch*$^{+}$, *MOLecular ARCHlitecture Modeling Programm V7.05*; Technical University of Darmstadt: Darmstadt, Germany, 2002.
(53) Jack, K. H.; Wild, S. A. *Acta Crystallogr.* **1966**, *S21*, A81
(54) Stockwell, D. M.; Bianchi, D.; Bennett, C. O. *J. Catal.* **1988**, *113*, 13.
(55) Didziulis, S. V.; Butcher, K. D.; Perry, S. S. *Inorg. Chem.* **2003**, *42*, 7766.
(56) Soresu, D. C.; Yates, J. T., Jr. *J. Phys. Chem. B* **2002**, *106*, 6184.
(57) Gay, R. R.; Nodine, M. H.; Henrich, V. E.; Zeiger, H. J.; Solomon, E. I. *J. Am. Chem. Soc.* **1980**, *102*, 6752.
(58) Mulliken, R. S. *J. Chem. Phys.* **1955**, *23*, 1833.
(59) Segall, M. D.; Pickard, C. J.; Shah, R.; Payne, M. C. Population analysis in plane wave electronic structure calculations. *Mol. Phys.* **1996**, *89*, 571.
(60) Segall, M. D.; Shah, R.; Pickard, C. J.; Payne, M. C. Population analysis of plane wave electronic structure calculations of bulk materials. *Phys. Rev. B* **1996**, *54*, 16317.
(61) Blyholder, G. *J. Phys. Chem.* **1964**, *68*, 2772.
(62) Moon, D. W.; Bernasek, S. L.; Dwyer, D. J.; Gland, J. L. *J. Am. Chem. Soc.* **1985**, *107*, 4363.
(63) Moon, D. W.; Dwyer, D. J.; Bernasek, S. L. *Surf. Sci.* **1985**, *163*, 215.
(64) Dwyer, D. J.; Rausenberger, B.; Cameron, S. D.; Lu, J. P.; Bernasek, S. L.; Fischer, D. A.; Parker, D. H.; Gland, J. L. *Surf. Sci.* **1989**, *224*, 375.